Forcing Global Fire Emissions Database burned-area dataset into Community Land Model version 5.0: Impacts on carbon and water fluxes at high latitudes

Hocheol Seo [1], Yeonjoo Kim [1]

[1]Department of Civil and Environmental Engineering, Yonsei University, Seoul 03722, South Korea

Correspondence to: Yeonjoo Kim (yeonjoo.kim@yonsei.ac.kr)

Abstract. Wildfires influence not only ecosystems but also carbon and water fluxes on Earth. Yet, the fire processes are still limitedly represented in land surface models (LSMs), thus simulating the occurrence and consequences of fires. Especially, the performance of LSMs in estimating burned areas across high northern latitudes is poor. In this study, we employed the daily burned areas from satellite-based Global Fire Emission Database (version 4) (GFED4) into Community Land Model (version 5.0), with a biogeochemistry module (CLM5-BGC) to identify the effects of accurate fire simulation on carbon and water fluxes over Alaska and Eastern Siberia. The results showed that the simulated carbon emissions with burned areas from GFED4 (i.e., experimental run) were significantly improved in comparison to the open-loop run (that is default run), which resulted in opposite signs of the net ecosystem exchange for 2004, 2005, and 2009 over Alaska between the default and experimental runs. Also, we identified carbon emissions were more sensitive to the wildfires in Alaska than in Eastern Siberia, which could be explained by the vegetation distribution (i.e., tree cover ratio). In terms of water fluxes, canopy transpiration in Eastern Siberia was relatively insensitive to the size of burned area due to the interaction between leaf size and soil moisture. This study uses CLM5-BGC to improve our understanding of the role of burned areas in eco-hydrological processes at high latitudes. Furthermore, we suggest that the improved approach will be required for better predicting future carbon fluxes and climate change.

1 Introduction

Wildfires are natural phenomena that directly and indirectly affect the life of humans as well as vegetated ecosystems (Bowman et al., 2009; Haque et al., 2021; Holloway et al., 2020; Li et al., 2017). Wildfires burn the leaves, stems, and roots of plants and alter ecological communities, which is called secondary succession (Knelman et al., 2015; Metrak et al., 2008; Seo and Kim et al., 2019). Moreover, annual carbon emissions from wildfires were estimated to be approximately 2.1 Pg, which affects the global carbon cycle (Arora and Melton et al., 2018; van der Werf et al., 2010). Wildfires can be a potential disaster that result in enormous damage; for example, the damage costs of Australian wildfires from 2019 to 2020 was estimated to be over $100 billion, covering infrastructure damage, job losses, and firefighting cost (Deb et al., 2020). Moreover, the smoke particles from wildfires may be harmful to human health (Cascio, 2018; Black et al., 2017).

1

서식 지정함: 영어(영국)

삭제함: – Biogeochemistry

삭제함: the

삭제함: global fire emission database

삭제함: the community land model

삭제함:)

삭제함: the

삭제함: i.e.,

삭제함: trends

삭제함: open-loop

삭제함: remarkably

40

Especially, in high latitudes areas, such as boreal forest and tundra regions, the wildfire intensity and occurrence have increased over the past decades (Jiang et al., 2015; Madani et al., 2021; Veraverbeke et al., 2017). While few arctic fires had occurred historically because of the low temperatures in summer season, snow cover, and short growing seasons, arctic fires are no longer unusual owing to warming trends. For instance, unprecedented large fires (more than 1.5 Mha of burned areas) in

45 interior Alaska were reported in 2004 and 2015. From these fires, more than 50 Tg C was emitted, according to the Alaskan Fire Emissions Database (AKFED) (Veraverbeke et al., 2015). These fires not only result in carbon emissions from vegetation but also increase the soil temperature in summer, which could induce permafrost thawing (Holloway et al., 2020; Jiang et al., 2015). This could result in the release of belowground carbon, which can increase the levels of carbon dioxide in the atmosphere.

50

Fires at high latitudes are primarily ignited by natural processes rather than by humans. Veraverbeke et al. (2017) reported that 76–87% of fire ignition and 82–95% of burned areas were the result of the lightning occurring between 1975 and 2015 in North American boreal forests. They also suggested that persisting warming and dryness accelerate the spread of fires, which could cause extreme fires. Furthermore, their regression analysis showed that lightning frequency will increase in the future

55 (2050–2074), which may increase the burned area in Alaska. Therefore, understanding the fire mechanism is critical to predict future fires and carbon emissions as well as evaluate the fire risk to permafrost carbon.

To understand and describe wildfire dynamics, many fire models such as Community Land Model (CLM)-Li (Li et al., 2012), SPread and InTensity of FIRE (Thonicke et al., 2010), MC-Fire (Conklin et al., 2015), Fire Including Natural & Agricultural

60 Lands model (Rabin et el., 2018), and the interactive fire and emission algorithm for natural environments (Mangeon et al., 2016), which have been incorporated into earth system models (ESMs) and land surface models (LSMs), have been developed. As individual fire models were developed for different purposes, each model calculates fire ignition, burned area, fire combustion, and mortality based on different structures of fire regime and input data. The Fire Modeling Intercomparison Project (FireMIP; Rabin et el., 2017) was executed for comparing the performances of these fire models and assessing their

65 strengths and weaknesses in details. Despite these efforts of developing fire models, LSMs are still limited in representing the burned area thus simulating fire impacts on the land surface processes. This is because understanding of a process-based fire mechanism remains elusive and thus large uncertainties of fire parameterization exist (Wu et al., 2021).

In this study, we aimed to understand the significance of fire prediction in further simulating fire impacts on ecohydrological

70 processes in the LSMs. We implemented the daily burned areas derived from Global Fire Emissions Database (GFED) for twelve years (2001–2012) over the arctic region into the National Center for Atmospheric Research (NCAR) CLM version 5.0 with a biogeochemistry module (CLM5-BGC), one of the widely used LSMs. In CLM5-BGC, the burned area is predicted based on the empirical relationships among lightning frequency, human population density and vegetation composition, which

2

삭제함: at

삭제함: carbon in

삭제함: regions

삭제함: 2016

is limited in capturing the observed burned areas from the GFED over several areas, including those at high latitudes. We compared the results of the default CLM5-BGC simulation (hereafter, CLM-Default, which uses the default fire module) and the experimental simulation with GFED4 (hereafter, EXP-GFED4) with a focus on Alaska and Siberia, where there are large uncertainties of fire prediction (i.e., prediction of burned area). Furthermore, we examined the simulated carbon fluxes and water fluxes, including evapotranspiration (ET) and soil moisture in CLM-Default and EXP-GFED4.

2 Methods

2.1 Model description

CLM5, a land component of the NCAR Community Earth System Model (version 2.0.1), is a grid-based computational model (Lawrence et al., 2019). Each grid cell comprises of sub-grids that represent the land cover type (i.e., glacier, lake, wetland, urban, and vegetated). The 17 plant functional types (PFTs) are represented in the vegetated land cover. The model represents the instantaneous exchange of energy, and water and momentum were simulated between terrestrial and atmosphere across a variety of spatial and temporal scales at the sub-grid level. Furthermore, hydrological processes including evapotranspiration, surface runoff, sub-surface runoff, stream flow, aquifer recharge, and snow are simulated at the sub-grid level. When the BGC module is adopted (i.e., CLM5-BGC), the carbon and nitrogen cycles and seasonal vegetation phenology are simulated for the atmosphere, vegetation, and soil organic matter at the PFT-level. These cycles, which are linked to climate, land cover and land use, fires, and atmosphere CO_2 level, affect other cycles such as hydrological cycles and energy fluxes.

In CLM5-BGC, fire is simulated based on a process-based fire parameterization developed by Li et al. (2012). There are four types of fire in CLM5-BGC: non-peat fire, agriculture fire, deforestation fire, and peat fire. For non-peat fires, the number of fire ignitions is calculated as the sum of natural and anthropogenic ignitions. The estimation of natural ignition sources is based on the NASA Lightning Imaging Sensor (LIS) / Optical Transient Detector (OTD) lightning frequency datasets. The frequency of cloud-to-ground lightning that ignite fires is estimated with the latitudinally varying ratios of total lightning frequency obtained from remotely sensed data (i.e., LIS/OTD), which include two different types of lightning, i.e., cloud-to-ground and the cloud-to-cloud lightning. Furthermore, the ignition source from human activity is calculated based on the human population density. The fire spread rate is then calculated by considering wind speed and vegetation condition (Arora and Boer, 2005). Socioeconomic influences are parameterized using GDP and population density, which means that higher populated and more developed regions will have a better fire suppression capacity.

In CLM, the burned area is calculated at the grid level and the fire emissions are calculated at a PFT level. Once a grid-level burned area is calculated, the same fractional area burned is imposed on each PFT in the grid. The PFT-level carbon emission from the fire is calculated as follows (24.26 in Lawrence et al., 2019):

3

$$CE = A \cdot C \cdot CC \qquad (1)$$

where CE is the carbon emission; A is the fractional area burned; C is a vector with the carbon density of leaves, stems, and roots, carbon transfer, and carbon pools; and CC is the corresponding combustion completeness factor vector.

Leaves and roots may be damaged in burned areas, which reduces their carbon-capturing productivities (Reyer et al., 2017; Seo and Kim, 2019; Swezy and Agee, 1991). In CLM5-BGC, the amount of leaf carbon to litter (Ψ) caused by fire is calculated as follows (24.27 in Lawrence et al., 2019):

$$\Psi = \frac{A_b}{f_i \cdot A_g} \cdot C_{leaf}(1 - CC) \cdot M \qquad (2)$$

where A_b is the calculated burned area, A_g is the area of the grid cell, f_i is the fraction of coverage of each PFT, C_{leaf} is the amount of leaf carbon, and M is the mortality factor vector for each PFT. The leaf area index (LAI) is recalculated based on the adjusted amount of leaf carbon. In addition, the methods by which the amount of carbon in live stems, dead stems, and roots and the storage pool are adjusted due to fires are similar to those mentioned above.

Leaf size controls canopy evaporation and transpiration as well as carbon fluxes (gross primary production (GPP), net primary production (NPP), net ecosystem production (NEP), and net ecosystem exchange (NEE)). NEE, which represents the total carbon fluxes between an ecosystem and the atmosphere, is calculated by using the NEP and carbon emissions from wildfires. The equations for these carbon fluxes are as follows:

$$NPP = GPP - R_p \qquad (3)$$

$$NEP = NPP - R_h \qquad (4)$$

$$NEE = -NEP + CE \qquad (5)$$

where R_p is plant respiration and R_h is heterotrophic respiration.

Because hydrological processes are highly linked to vegetation dynamics, fire processes may affect not only water cycles but also ecosystem products (Jiao et al., 2017). For instance, the water cycles on land surfaces, such as partitioning of ET, are affected by fires because the fire changes leaf area in ecosystems (Netzer et al., 2009; Park et al., 2020; Seo and Kim, 2019;

삭제함: $\Psi = \frac{A_b}{f_i \cdot A_g} \cdot C_{leaf}(1 - CC) \cdot M \rightarrow \rightarrow \rightarrow (2)$

삭제함: Especially, the

삭제함: represent

삭제함: $NPP = GPP - R_p$

서식 지정함: 글꼴: 굵게

삭제함: $NEP = NPP - R_h$

서식 지정함: 글꼴: 굵게

삭제함: $NEE = -NEP + CE$

서식 지정함: 글꼴: 굵게

삭제함: size

Wang et al., 2019). More details on CLM5-BGC processes, including the equations for leaf phenology, hydrology cycles, fires,

160 and carbon cycles, are described in Lawrence et al. (2019).

2.2 Site description

In this study, we focused on Alaska (200° E–218° E, 61° N–70° N) and Eastern Siberia (130° E–148° E, 61° N–70° N), which are located at northern high latitudes (Figure 1). Both domains have the same size and latitudes. The average temperature based on CRU-NCEP reanalysis data (2001–2012) is -5.11 and -15.28 degrees Celsius in Alaska and Eastern Siberia, respectively.

165 The average annual snowfall and rainfall are 83 mm and 218 mm in Alaska and 92 mm and 208 mm in Eastern Siberia, respectively.

There are differences in vegetation types in these regions, based on MODIS (Sun et al., 2008) (evergreen trees: 26.4%, deciduous trees: 1.6%, shrub: 28.5%, grass: 34.5%, crop: 3.9%, and bare ground: 5.1% in Alaska: evergreen trees: 1.2%,

170 deciduous trees: 14.9%, shrub: 45.8%, grass: 29.7%, crop: 1.4%, and bare ground: 7.1 % in Eastern Siberia). In summary, the tree fraction is higher in Alaska (28%) than that in Eastern Siberia (16.1%), and the fraction of low vegetation (i.e., grasses and shrubs) is lower in Alaska (63%) than that in Eastern Siberia (74.5%). Notably, the largest areas were the natural vegetation and crop land units, and the lake, urban, and glacier land units occupied less than 1% in both regions.

2.3 Experimental design

175 In this study, we designed two sets of experiments to investigate the impact of burned area using fire simulation based on the study by Li et al. (2012) (i.e., CLM-Default) and satellite observations from GFED4 (i.e., EXP-GFED) to investigate the fire impact on the terrestrial model for Alaska and Eastern Siberia. CLM-Default and EXP-GFED4 were simulated at a spatial resolution of 0.5 longitude and 0.5 latitude using Climate Research Unit (CRU) – National Centers for Environmental Prediction (NCEP) reanalysis climate data, which include precipitation, temperature, wind speed, surface pressure, specific

180 humidity, longwave radiation, and solar radiation. Figure 2 shows the spin-up simulation, which stabilizes the land state, including the LAI, soil moisture, and soil temperature, with the initial file of the year 2000 in the equilibrium state. It was repeatedly run for 200 years using 20-year CRU/NCEP forcing data for 1980–2000 before adopting CLM-Default and EXP-GFED4. While burned areas were simulated based on Li et al. (2012) in CLM-Default, the GFED daily burned area over the arctic region was directly inserted into CLM5-BGC in EXP-GFED4, with the daily data being equally divided into a half-

185 hourly model timestep (Seo and Kim, 2022).

In this study, we compared the carbon and water fluxes in CLM-Default and EXP-GFED4. Especially, carbon emissions and the NEE were evaluated using the GFED database, AKFED, and GEOS-Carb CASA-GFED. Additionally, we analyzed the impacts of fire on carbon fluxes according to the distribution of PFT. Furthermore, comparisons of water fluxes such as ground

5

evaporation, canopy evaporation, canopy transpiration, and soil moisture at grid level were performed to reveal the impacts of fire on water cycles.

265 **2.4 Fire and carbon fluxes datasets**

The GFED (version 4), which is based on satellite data such as MODIS and Tropical Rainfall Measuring Mission Visible and Infrared Scanner, provides gridded data on global burned area, fire persistence, land cover distribution, and fractional tree cover distribution of burned areas, among others (Giglio et al., 2013). The data are provided at a 0.25° × 0.25° resolution and daily and monthly temporal resolutions. Furthermore, details on fire impacts, such as carbon emissions, dry matter emissions,

270 biosphere fluxes (NPP, heterotrophic respiration) and emission factors data are included. The carbon emission data are based on burned areas and the Carnegie-Ames-Stanford Approach (CASA) carbon-cycle terrestrial model for each month. In this study, daily burned area data from GFED4 were incorporated into CLM5-BGC, and monthly scaled carbon emission data from GFED4 were used to evaluate the model performance (Table 1).

275 We also used data on Alaskan carbon emissions from the AKFED (Veraverbeke et al., 2015) to evaluate the model performance for carbon emissions in Alaska (Table 1).Veraverbeke et al. (2015) developed a statistical model to calculate the carbon

consumption in Alaska between 2001 and 2012. They employed environmental variables such as elevation, slope, and day of burning to calculate ground-level carbon consumption. In addition, pre-fire tree cover and differenced normalized burn ratio are used to predict above ground carbon emission. They estimated that the highest carbon emission was 69 Tg C in 2004 and

280 the annual carbon emission was 15 Tg C.

We used monthly NEE products from GEOS-Carb CASA-GFED for 2003 to 2012 to evaluate the performance of EXP-GFED4 and CLM-Default. However, the definitions of NEE according to CLM5-BGC and GEOS-Carb CASA-GFED are quite

different. In CLM5-BGC, the NEE is the final carbon flux between an ecosystem and the atmosphere. Thus, the carbon flux of burning was included when calculating the NEE (Eq. 5), but it was excluded in GEOS-Carb CASA-GFED. To unify the

285 definition of NEE, we redefined the NEE in GEOS-Carb CASA-GFED as follows.

$$NEE = NEE_{ge} + FireE + FuelE \qquad (6)$$

290 where NEE is the total carbon flux between terrestrial and atmosphere including emission dues to fires, NEE_{ge} is the value of NEE according to GEOS-Carb CASA-GFED, $FireE$ is the wildfire carbon emissions, and $FuelE$ is the carbon emissions from wood-fuel burning in GEOS-Carb CASA-GFED.

3 Results

3.1 Burned area

We first evaluated the performance of estimating burned areas in Alaska and Eastern Siberia from CLM5-BGC (i.e., CLM-Default) and compared it to that of GFED4 (Figure 3). While an average of 0.42 Mha of burned area from 2001 to 2012 was observed in Alaska, the average of annual burned area was estimated at 0.24 Mha in CLM-Default (Figure 3a). In Alaska, there were large discrepancies of burned areas for 2004, 2005, and 2008 between the GFED4 and simulation results. More than 1 Mha of burned area existed for three years (2004, 2005, and 2009), which is remarkably different from that of the other years. Studies suggested that these large burned areas were associated with a high lightning frequency and drought (Littell et al., 2016; Veraverbeke et al., 2017; Xiao and Zhuang, 2007;). However, this phenomenon was not captured in CLM5-BGC, which predicts relatively constant annual burned areas. In contrast, the burned area was dramatically overestimated in Eastern Siberia (Figure 3b). While an average of 0.29 ha of burned area was observed, the average of annual burned area was estimated at 2.14 ha with CLM5-BGC. Although the GFED burned area in Eastern Siberia did not vary significantly over time, the simulated burned area increased from 2001 to 2012 at a rate of 0.33 Mha/year.

Figure 4 shows the spatial distribution of the burned areas of GFED4 and CLM-Default in 2004 over Alaska. The number of grid cells (0.5 × 0.5 degree) in CLM-Default where the burned areas exceeded 0.1 ha in 2004 was more than 50. In contrast to the GFED4 burned areas, there were two grid cells with more than 0.1 ha of burned areas simulated using CLM5-BGC in Alaska (Table 2). Table 2 shows that CLM5-BGC has a limitation in simulating large burned areas in Alaska. Small fires were simulated in more grid cells, and the simulated burned areas were more widely distributed than those in the GFED4 products.

3.2 Fire impacts on carbon fluxes

We compared the carbon fluxes of CLM-Default and EXP-GFED4 to understand the impacts of fire on high latitudes regions (Figure 5 and 6 and Table 3). The average carbon emissions were 11.87 and 21.11 g m^{-2} year^{-1} in CLM-Default and EXP-GFED4 in Alaska, respectively, and 20.48 and 3.24 g m^{-2} year^{-1} in CLM-Default and EXP-GFED4 in Eastern Siberia, respectively (Table 3). As expected, there were large differences in carbon emissions in CLM-Default and EXP-GFED4 in both regions because the simulated carbon emission was directly linked to burned areas. In the model, carbon emissions had a strong correlation with burned areas in both regions (Alaska: 0.99, Eastern Siberia: 0.89).

Furthermore, the simulated Alaskan annual carbon emission for CLM-Default and EXP-GFED4 were evaluated with AKFED carbon emission datasets and GFED4 (Figure 5a and Table 4). The correlations of annual carbon emission between simulated carbon emissions (CLM-Default and EXP-GFED4) and GFED4 were 0.3 and 0.99, respectively. Moreover, the correlations between the simulated carbon emissions and AKFED carbon emissions were determined (CLM-Default: 0.31 and EXP-

7

GFED4: 0.96). While the root mean square error (RMSE) between the simulated carbon emissions and the AKFED carbon emissions decreased (CLM-Default: 20.48 g m^{-2} year^{-1} and EXP-GFED4: 10.98 g m^{-2} year^{-1}), the RMSE between the simulated carbon emissions and the GFED4 carbon emissions increased (CLM-Default: 11.02 g m^{-2} year^{-1} and EXP-GFED4: 20.93 g m^{-2} year^{-1}). This is because average carbon emissions for GFED4 were 8.36 g m^{-2} year^{-1} and are relatively lower than carbon emissions in EXP-GFED4 and AKFED. The combustion completeness factor for leaves is 0.8 and that for stems ranges from 0.27–0.8, depending on the PFTs in CLM5-BGC. According to van der Werf et al. (2010), the combustion completeness factor of aboveground live biomass, which ranges from 0.3–0.4 in the boreal region, is lower than that in other regions. Therefore, the combustion completeness factors for boreal trees may be lower than the current default value in CLM5-BGC.

The carbon emission simulation was highly improved after replacing the fire simulation with GFED4 in Eastern Siberia (Figure 5b); the correlation was improved from 0.41 in CLM-Default to 0.88 in EXP-GFED4, and the RMSE was reduced from 19.74 g m^{-2} year^{-1} in CLM-Default to 4.2 g m^{-2} year^{-1} in EXP-GFED4, compared with the GFED4 products. *In Eastern Siberia, grasses are dominant, suggesting that the value of the combustion completeness factors for grass in CLM5-BGC is more similar to those of GFED4 products than to those of boreal trees.*

Unlike carbon emissions, the regionally-averaged GPP, NPP, and NEP (Figure 6c–6h) did not significantly change in EXP-GFED4. The differences in GPP, NPP, and NEP are less than 3%, indicating that fires rarely impacted carbon fluxes related to vegetation and decomposition. This is because the ratio of the fire area to the total area was relatively small. For example, the highest annual burned area of all simulations was 6 Mha, which accounted for 6.87% of our study domain. The simulated LAIs in Alaska and Eastern Siberia are presented in Figure 6a and 6b, respectively. In Alaska (Figure 6a), the difference in LAI between CLM-Default and EXP-GFED4 was the largest in 2005 (0.03 m2/m2). Although the difference in burned area between CLM-Default and GFED4 (Figure 3a) was the largest in 2004, the largest difference in LAI was in 2005 since vegetation damage caused by fire in 2004 had not fully recovered, and the difference in burned area in 2005 was also quite large. In Eastern Siberia (Figure 6b), the difference in the simulated LAI between CLM-Default and EXP-GFED4 has been large since 2009, when the difference in the size of burned areas was amplified (Figure 3b). Although the LAI, which affects primary GPP and other carbon fluxes, was reduced by fires, the LAI after fires was not substantially different owing to the small fire area compared to the total area.

However, NEE, which represents the net carbon fluxes between terrestrial and ecosystem (Eq. 5), was largely affected by fires, unlike other fluxes such as GPP, NEE, and NEP (Figure 5c and 5d). NEE changed significantly with forcing of GFED4 into the model when the discrepancy of burned area between CLM-Default and EXP-GFED4 was remarkable. Moreover, the NEE results for EXP-GFED4 and GEOS-Carb CASA-GFED had similar tendencies. For instance, we found that the net carbon in Alaska was emitted from land ecosystems to the atmosphere (i.e., positive NEE) in 2004, 2005, and 2009 in EXP-GFED4 and

GEOS-Carb CASA-GFED, but it was absorbed (i.e., negative NEE) in CLM-Default. Although there was a change in NEE due to burned areas in Siberia, it was not as pronounced as that in Alaska.

The results of the carbon fluxes at the grid level in Alaska and Eastern Siberia are investigated in Figure 7, which shows the difference of carbon fluxes and burned areas between CLM-Default and GFED4 in Alaska for 2004 and in Eastern Siberia for 2012. As expected, the response of GPP, NPP, and NEP to fires were nonsignificant. However, fires significantly altered carbon emissions and the NEE in both regions, which can further alter the atmospheric carbon dioxide concentration and even climate. This suggests that high-latitudes fires may influence the carbon sink or uptake markedly. Phillips et al. (2022) reported that boreal forest fires, which are largely distributed at high latitudes, make a significant contribution to releasing greenhouse gases. With the earth system model combined with CLM5-BGC, the prediction of atmospheric carbon may become uncertain due to the limited performance of fire prediction models.

3.3 Fire impacts on water fluxes

To investigate the fire impacts on water fluxes, we compared the results of ET and ET components, such as canopy evaporation, canopy transpiration, and ground evaporation, in six grid cells where the differences in burned area between CLM-Default and EXP-GFED4 are the largest in Alaska and Eastern Siberia (Figure 8). Because the LAI decreases owing to wildfires, canopy evaporation and canopy transpiration decrease in the burned areas.

We observed that more rainfall reaches the ground, which would make the ground evaporation rate higher in regions with more burned areas, especially in 2004 and 2005 in Alaska. The differences in annual canopy evaporation, canopy transpiration, and ground evaporation between the two simulations were 5.41 mm and 13.37 mm, 2.3 mm and 6.26 mm, and -1.39 mm and -7.4 mm in 2004 and 2005, respectively. Canopy transpiration decreased by 3%, canopy evaporation decreased by 12%, and ground evaporation increased by 10% in 2004 and 2005 after applying the GFED4 burned area into CLM. This is consistent with the findings of Li et al. (2017) and Seo and Kim (2019), showing that canopy evaporation and canopy transpiration decreased, and ground evaporation increased, when comparing the simulation with and without fire. Furthermore, the total ET in the presence of fire decreased by 6.32 mm and 12.08 mm in 2004 and 2005, respectively, indicating that canopy evaporation is more strongly influenced by fires over Alaska in CLM.

In Eastern Siberia, the patterns of canopy evaporation and ground evaporation were the same as those of Alaska. Canopy evaporation increased and ground evaporation decreased in EXP-GFED4 because the simulated burned area decreased, which was noticeable from 2009 to 2012 (Figure 9f and 9h). However, the canopy transpiration of EXP-GFED4 was similar to that of CLM-Default. In other words, there was no significant change in canopy transpiration due to a change in burned area. Furthermore, the ET with the burned area applied changed slightly in Eastern Siberia. Differences in the average canopy

evaporation and ground evaporation were -9.19 mm (28%) and 6.97 mm (10%) from 2009 to 2012, respectively. The reasons for the smaller change in canopy transpiration is related to soil moisture and leaf size.

Figure 9 shows differences in the simulated soil moisture for CLM-Default and EXP-GFED4 at 0–20 cm (hereafter top soil) and 70–150 cm (hereafter bottom soil) in both regions. In Eastern Siberia, the top soil moisture and bottom soil moisture decreased after applying the observed burned areas. Although the leaf size increased with less burned areas applied, transpiration did not change significantly due to the decreased soil moisture. On the contrary, there was no considerable difference in the top and bottom soil moisture between CLM-Default and EXP-GFED4. Therefore, transpiration was positively correlated with leaf size. According to the McVicar et al. (2012) and Nemani et al (2003), the Alaska region is drier and more water-limited than Eastern Siberia. Energy is sufficient to evaporate the increased stored water from the ground, which explains why soil moisture did not change considerably in Alaska.

4 Discussions

Difference in burned area between the model and observation may be attributed to incorrect input data such as lightning frequency and fire management as well as a misrepresentation of fire processes. First, the limited representation of fire ignition sources and spread may create discrepancies between modeled and observed burned areas. Lightning, which is a major source of fire at high latitudes, especially in Alaska, has increased because of the warming climate (Kepski and Kubicki, 2022). Although the lightning frequency at high latitudes varied yearly, the climatology of the 3-hourly lightning frequency from 1995 to 2011 was used in CLM. Moreover, the calculated ratio of cloud-to-ground lightning has large uncertainties and may cause models to misestimate fire ignition and burned areas. Furthermore, it is inherent that the grid-based large-scale model is limited in capturing micro-environmental impacts on fire spread. Fires spread differs depending not only on the temperature, precipitation, wind speed, and direction but also on the composition of vegetation at the local scale.

In addition, wildfires are strongly affected by the weather conditions after the fire ignition. For example, wind and precipitation determine the spread and duration of fire. However, in CLM5-BGC, the fire ignition and fire spread rate are simultaneously calculated based on the weather conditions of fire ignition or pre-fire. Moreover, wildfires in ecosystems persist from hours to months, depending on ecosystem characteristics and climate conditions. However, the duration of each fire is assumed to be equal to one day in CLM5-BGC (Li et al., 2012). For example, Andela et al. (2019) reported that the average fire duration in a boreal forest was longer than those in other regions, and the average size of each fire in the boreal forest was larger than those in temporal forests and under deforestation. Moreover, wind speed is an important factor determining fire spread in the model. In CLM, the spread of fire increases as the wind speed increases. However, according to Lasslop et al. (2015), there is strong variation in the burned fraction with wind speed, characterized by an increase until a certain wind speed threshold is

reached and a decrease thereafter. The study suggests that global fire models should avoid a strong amplification for higher wind speeds to prevent overestimation of modelled burned areas.

The management system and infrastructures for fires vary by country or region. For instance, there are four types of fire policy options in Alaska, namely critical, full, modified, and limited, according to the levels of anthropogenic effort in extinguishing the fire (Phillips et al., 2022). For example, fire suppression is the highest priority at the critical protection level because wildfire can threaten human life and inhabited property. The lowest priority for fire-related resource assignments is applied at the limited protection level. In Alaska, areas under the full, modified, and limited management options occupy 16%, 16%, and 67% of Alaska, respectively. Critical-protection-level areas occupy less than 1% of Alaska. In CLM5-BGC, however, the suppression impact is calculated based on the GDP and population, which may underestimate burned areas in the limited regions of Alaska because of the large GDP of the United States.

Moreover, inaccurate coverage of peatland can also cause a bias in burned area calculations. Peat fire and along with smouldering fire have been reported over both regions for several years (Scholten et al., 2021). However, peat fire was barely simulated in CLM-BGC5 because the fractions of peatland, which were derived from three datasets (Olson et al., 2001; Tarnocai et al., 2011; Lehner and Döll, 2004), were low over both regions. (Alaska: 0%, Eastern Siberia: 2%). On the contrary, several studies reported that there is sufficient coverage of peatland in both areas to consider the existence of peatland fires (Yu et al., 2010; Qiu et al., 2019). For instance, the coverage of peatland is 72–168 103km2, and 16–32 Pg of carbon is stocked in peatland in Alaska. Therefore, to simulate peat fires accurately, an improvement of the dataset used for peatland coverage in CLM should be considered.

Impact on carbon fluxes were further examined. Figure 10 shows the responses of carbon flux to changes in the burned area. The average change rates (difference in carbon fluxes/difference in burned area) of GPP, NEP, and NPP were -97.69, -5.12, and -32.27 gC ha^{-1} and -55.72, 32.83 and 26.55 gC ha^{-1} in Alaska and Eastern Siberia, respectively. The NPP was slightly positively correlated with fires because plant respiration is more sensitive compared to GPP in Eastern Siberia. In other words, if the burned area increases, both GPP and plant respiration will decrease. As plant respiration decrease more than GPP, it was simulated that NPP increases with the frequency of fires in Eastern Siberia with CLM-BGC5.

The average change rates of NEE and carbon fluxes were 4914 gC ha^{-1} and 4881 gC ha^{-1} and 771 gC ha^{-1} and 798 gC ha^{-1} in Alaska and Eastern Siberia, respectively. The response of carbon emissions to fires was much more sensitive than those of GPP, NPP, and NEP; therefore, changes in carbon emissions are a major cause of the change in the NEE, which is consistent with previous results. Carbon release owing to wildfires was more sensitive in Alaska than Eastern Siberia under CLM5-BGC, as boreal trees are more distributed in Alaska than in Eastern Siberia. Based on the above results, we suggest that more accurate fire predictions are needed to understand ecosystem carbon fluxes, especially in Alaska.

11

Therefore, one can tell that the carbon fluxes were more sensitive in Alaska than in Eastern Siberia. The reasons for carbon emissions being more pronounced in Alaska than in Eastern Siberia could be explained by the vegetation distribution. The average ratio of carbon emissions to burned areas was 49.98 Tg Mha^{-1} in Alaska and 9.76 Tg Mha^{-1} in Eastern Siberia. There was 95 Tg of leaf carbon and 8.3 Tg of live-stem carbon in Alaska and 29 Tg of leaf carbon and 2.4 Tg of live-stem carbon in Eastern Siberia in averages of CLM-Default and EXP-GFED4. Trees have a larger LAI and stems and thus more fuel combustibility and availability. Therefore, the ratio of carbon emissions to burned areas was high in forests than in grassland. Moreover, the final carbon fluxes between the atmosphere and vegetation were closely linked not only with vegetation metabolism but also with burned area and plant type. As the same fractional area burned is imposed on each PFT in a grid, the simulated carbon emission could differ from observed carbon emissions. For example, when an observation of forest fire is applied to CLM5-BGC, the fractional area burned is imposed on both grasses and trees in the same grid, causing biases in the carbon emission values. Therefore, a reasonable method of imposing grid-level burned areas into the PFT level is required.

5 Conclusions

In this study, we applied the daily burned area of GFED4 into CLM5-BGC over Alaska and Eastern Siberia. As the capacity of predicting the burned area with CLM5-BGC in high latitudes is poor, the simulated burned area was overestimated in Eastern Siberia, and it was underestimated in Alaska. Such model discrepancy could lead to misunderstanding of terrestrial carbon and water fluxes. By comparing our experiments of CLM-Default and EXP-GFED4 in Alaska and Eastern Siberia, we identified the effects of accurate fire simulation on carbon fluxes over Alaska and Eastern Siberia. While GPP, NPP, and NEP were not significantly affected by burned area, carbon emissions changed considerably in both regions; thus, NEE was significantly influenced by the burned area. Furthermore, carbon emissions were remarkably improved after applying GFED4 into CLM5-BGC, which caused opposite trends of simulated NEE between the CLM-Default and EXP-GFED4 for 2004, 2005, and 2009 in Alaska. In addition, the density of leaf and stem carbon in Alaska were much higher than those in Siberia, indicating that carbon emissions from fire in Alaska are more sensitive than those in Siberia.

Furthermore, while analysis of burned area impact on water fluxes showed that canopy evaporation and ground evaporation were changed consistently by fires, canopy transpiration and soil moisture were affected by the region. For example, canopy transpiration in Eastern Siberia was almost the same for CLM-Default and EXP-GFED4, because the leaf size was larger and soil moisture decreased due to reduced fires. However, the transpiration of EXP-GFED4 decreased as the leaf size was smaller but there was no significant change in soil moisture in Alaska. This may have been because Alaska is a more water-limited region; thus, energy is sufficient to evaporate the increased stored water from the ground. Although an accurate estimation of carbon cycles is necessary to predict the future climate, we found that the fire model was limited in representing burned areas

and, thus, in simulating carbon emissions and the NEE. Therefore, we suggest that innovative methods for simulating burned areas (i.e., using machine learning) should be required to better predict future carbon fluxes and climate change.

700 **Code and Data Availability**

CLM5, a land part of CESM 2.0.1, is available on GitHub at https://github.com/escomp/cesm.git (git tag: release-cesm2.0.1 last access: 20 December 2022). GFED4 products are available at https://daac.ornl.gov/VEGETATION/guides/fire_emissions_v4_R1.html. Carbon emissions database from AKFED and was available at https://daac.ornl.gov/CARVE/guides/AKFED_V1.html. NEE products from GEOS-Carb CASA-GFED were

705 available at https://disc.gsfc.nasa.gov/datasets/GEOS_CASAGFED_3H_NEE_3/summary. The revised codes, which enable the application of GFED4 into CLM5-BGC, are achieved on Zenodo at https://zenodo.org/record/7483115 (Seo and Kim, 2022).

Author contributions

HS and YK designed the study, and HS performed the model development, simulations, and result analysis under the

710 supervision of YK. HS wrote the original manuscript, and YK reviewed and edited the manuscript.

Competing interests

The authors declare that they have no conflict of interest.

Acknowledgements

13

References

Arora, V. K., and Boer, G. J.: Fire as an interactive component of dynamic vegetation models, Journal of Geophysical Research: 720 Biogeosciences, 110, G02008, https://doi.org/10.1029/2005jg000042, 2005.

Arora, V. K., and Melton, J. R.: Reduction in global area burned and wildfire emissions since 1930s enhances carbon uptake by land, Nature Communications, 9(1), https://doi.org/10.1038/s41467-018-03838-0, 2018.

Black, C., Tesfaigzi, Y., Bassein, J. A., and Miller, L. A.: Wildfire smoke exposure and human health: Significant gaps in research for a growing public health issue, In Environmental Toxicology and Pharmacology, 55, 186-195, 725 https://doi.org/10.1016/j.etap.2017.08.022, 2017.

Bowman, D., Balch, J., Artaxo, P., Bond, W., Carlson, J., Cochrane, M., Antonio, C., Defries, R., Doyle, J., Harrison, S., Johnston, F., Keeley, J., Krawchuk, M., Kull, C., Marston, J., Moritz. M., Prentice,I., Roos, C., Scott, A., Swetnam, T., van der Werf, G., and Pyne, S.: Fire in the Earth System, Science, 324, 481–484, https://doi.org/10.1126/science.1163886, 2009.

Cascio, W. E.: Wildland fire smoke and human health, Sci. Total Environ., 624, 586–595, 730 https://doi.org/10.1016/J.SCITOTENV.2017.12.086, 2018.

Conklin, D. R., Lenihan, J. M., Bachelet, D., Neilson, R. P., and Kim, J. B.: MCFire Model Technical Description, Tech. Rep. Gen. Tech. Rep. PNW-GTR-926, Portland, OR, 2015.

Deb, P., Moradkhani, H., Abbaszadeh, P., Kiem, A. S., Engström, J., Keellings, D., and Sharma, A.: Causes of the Widespread 2019–2020 Australian Bushfire Season, Earth's Future, 8(11), https://doi.org/10.1029/2020EF001671, 2020.

735 Giglio, L., Randerson, J. T., and van der Werf, G. R.: Analysis of daily, monthly, and annual burned area using the fourth-generation global fire emissions database (GFED4), Journal of Geophysical Research: Biogeosciences, 118(1), 317–328, https://doi.org/10.1002/jgrg.20042, 2013.

Haque, Md. K., Azad, Md. A. K., Hossain, Md. Y., Ahmed, T., Uddin, M., and Hossain, Md. M.: Wildfire in Australia during 2019-2020, Its Impact on Health, Biodiversity and Environment with Some Proposals for Risk Management: A Review. 740 Journal of Environmental Protection, 12(06), 391–414, https://doi.org/10.4236/jep.2021.126024, 2021.

Holloway, J. E., Lewkowicz, A. G., Douglas, T. A., Li, X., Turetsky, M. R., Baltzer, J. L., and Jin, H.: Impact of wildfire on permafrost landscapes: A review of recent advances and future prospects, Permafrost and Periglacial Processes, 31(3), 371–382, https://doi.org/10.1002/ppp.2048, 2020.

Holloway, J. E., Lewkowicz, A. G., Douglas, T. A., Li, X., Turetsky, M. R., Baltzer, J. L., and Jin, H.: Impact of wildfire on 745 permafrost landscapes: A review of recent advances and future prospects. Permafrost and Periglacial Processes, 31(3), 371–382, https://doi.org/10.1002/ppp.2048, 2020.

Jiang, Y., Rocha, A. v., O'Donnell, J. A., Drysdale, J. A., Rastetter, E. B., Shaver, G. R., and Zhuang, Q.: Contrasting soil thermal responses to fire in Alaskan tundra and boreal forest, Journal of Geophysical Research: Earth Surface, 120(2), 363–378, https://doi.org/10.1002/2014JF003180, 2015.

14

750 Kępski, D., and Kubicki,M.: Thunderstorm activity at high latitudesobserved at manned WMO weather stations, International Journal of Climatology, 1–23. https://doi.org/10.1002/joc.7678KęPSKIANDKUBICKI23, 2022.

Knelman, J. E., Graham, E. B., Trahan, N. A., Schmidt, S. K., and Nemergut, D. R.: Fire severity shapes plant colonization effects on bacterial community structure, microbial biomass, and soil enzyme activity in secondary succession of a burned forest, Soil Biology and Biochemistry, 90, 161–168, https://doi.org/10.1016/j.soilbio.2015.08.004, 2015.

755 Lawrence, D. M., Fisher, R. A., Koven, C. D., Oleson, K. W., Swenson, S. C., Bonan, G., Collier, N., Ghimire, B., van Kampenhout, L., Kennedy, D., Kluzek, E., Lawrence, P. J., Li, F., Li, H., Lombardozzi, D., Riley, W. J., Sacks, W. J., Shi, M., Vertenstein, M., Wieder, W. R., Xu, C., Ali, A. A., Badger, A. M., Bisht, G., van den Broeke, M., Brunke, M. A., Burns, S. P., Buzan, J., Clark, M., Craig, A., Dahlin, K., Drewniak, B., Fisher, J. B., Flanner, M., Fox, A. M., Gentine, P., Hoffman, F., Keppel-Aleks, G., Knox, R., Kumar, S., Lenaerts, J., Leung, L. R., Lipscomb, W. H., Lu, Y., Pandey, A., Pelletier, J. D., Perket,

760 J., Randerson, J. T., Ricciuto, D. M., Sanderson, B. M., Slater, A., Subin, Z. M., Tang, J., Thomas, R. Q., Val Martin, M., and Zeng, X.: The Community Land Model Version 5: Description of New Features, Benchmarking, and Impact of Forcing Uncertainty, J. Adv. Model. Earth Sy., 11, 4245–4287, https://doi.org/10.1029/2018MS001583, 2019.

Lehner, B. and Döll, P.: Development and validation of a global database of lakes, reservoirs and wetlands, J. Hydrol., 296, 1–22, https://doi.org/10.1016/j.jhydrol.2004.03.028, 2004.

765 Li, F., Lawrence, D. M., and Bond-Lamberty, B.: Impact of fire on global land surface air temperature and energy budget for the 20th century due to changes within ecosystems, Environmental Research Letters, 12(4), https://doi.org/10.1088/1748-9326/aa6685, 2017.

Li, F., Zeng, X. D., and Levis, S.: A process-based fire parameterization of intermediate complexity in a dynamic global vegetation model, Biogeosciences, 9(7), 2761–2780, https://doi.org/10.5194/bg-9-2761-2012, 2012.

770 Littell, J. S., Peterson, D. L., Riley, K. L., Liu, Y., and Luce, C. H.: A review of the relationships between drought and forest fire in the United States, Glob. Change Biol., 22, 2353–2369, 2016.

Madani, N., Parazoo, N. C., Kimball, J. S., Reichle, R. H., Chatterjee, A., Watts, J. D., Saatchi, S., Liu, Z., Endsley, A., Tagesson, T., Rogers, B. M., Xu, L., Wang, J. A., Magney, T., and Miller, C. E. The Impacts of Climate and Wildfire on Ecosystem Gross Primary Productivity in Alaska, Journal of Geophysical Research: Biogeosciences, 126(6),

775 https://doi.org/10.1029/2020JG006078, 2021.

Mangeon, S., Voulgarakis, A., Gilham, R., Harper, A., Sitch, S., and Folberth, G.: INFERNO: a fire and emissions scheme for the UK Met Office's Unified Model, Geosci. Model Dev., 9, 2685–2700, doi:10.5194/gmd-9-2685-2016, 2016

McVicar, T. R., Roderick, M. L., Donohue, R. J., Li, L. T., Van Niel, T. G., Thomas, A., Grieser, J., Jhajharia, D., Himri, Y., Mahowald, N. M., Mescherskaya, A. V., Kruger, A. C., Rehman, S., and Dinpashoh, Y.: Global review and synthesis of trends

780 in observed terrestrial near-surface wind speeds: Implications for evaporation, J. Hydrol., 416, 182–205, 2012.

Mętrak, M., Malawska, M., Kamiński, J., Błocka, A. and Wiłkomirski, B.: Plant secondary succession patterns after 2002 wildfire in the Biebrza National Park, Phytopedon, 7, 109–114, 2008.

15

Nemani, R. R., Keeling, C. D., Hashimoto, H., Jolly, W. M., Piper, S. C., Tucker, C. J., Myneni, R. B., and Running, S. W.: Climate-Driven Increases in Global Terrestrial Net Primary Production from 1982 to 1999, Science, 300, 1560–1563, https://doi.org/10.1126/science.1082750, 2003.

785

Netzer, Y., Yao, C., Shenker, M., Bravdo, B. A., and Schwartz, A.: Water use and the development of seasonal crop coefficients for Superior Seedless grapevines trained to an open-gable trellis system, Irrigation Science, 27(2), 109–120, https://doi.org/10.1007/s00271-008-0124-1, 2009.

Olson, D. M., Dinerstein, E., Wikramanayake, E. D., Burgess, N. D., Powell, G. V. N., Underwood, E. C., D'Amico, J. A.,

790

Itoua, I., Strand, H. E., Morrison, J. C., Loucks, C. J., Allnutt, T. F., Ricketts, T. H., Kura, Y., Lamoreux, J. F., Wettengel, W. W., Hedao, P., and Kassem, K. R.: Terrestrial Ecoregions of the World: A New Map of Life on Earth, BioScience, 51, 933–938, 2001.

Park, S. W., Kim, J. S., and Kug, J. S.: The intensification of Arctic warming as a result of CO2 physiological forcing, Nature Communications, 11(1), https://doi.org/10.1038/s41467-020-15924-3, 2020.

795

Phillips C A, Rogers B M, Elder M, Cooperdock S, Moubarak M, Randerson J T and Frumhoff P C 2022 Escalating carbon emissions from North American boreal forest wildfires and the climate mitigation potential of fire management, Sci. Adv., 8, https://www.science.org/doi/10.1126/sciadv.abl7161, 2022.

Qiu, C., Zhu, D., Ciais, P., Guenet, B., Peng, S., Krinner, G., Tootchi, A., Ducharne, A., and Hastie, A.: Modelling northern peatland area and carbon dynamics since the Holocene with the ORCHIDEE-PEAT land surface model (SVN r5488), Geosci.

800

Model Dev., 12, 2961–2982, https://doi.org/10.5194/gmd-12-2961-2019, 2019.

Rabin, S. S., Melton, J. R., Lasslop, G., Bachelet, D., Forrest, M., Hantson, S., Kaplan, J. O., Li, F., Mangeon, S., Ward, D. S., Yue, C., Arora, V. K., Hickler, T., Kloster, S., Knorr, W., Nieradzik, L., Spessa, A., Folberth, G. A., Sheehan, T., Voulgarakis, A., Kelley, D. I., Prentice, I. C., Sitch, S., Harrison, S., and Arneth, A.: The Fire Modeling Intercomparison Project (FireMIP), phase 1: experimental and analytical protocols with detailed model descriptions, Geosci. Model Dev., 10, 1175–1197,

805

https://doi.org/10.5194/gmd-10-1175-2017, 2017.

Rabin, S. S., Ward, D. S., Malyshev, S. L., Magi, B. I., Shevliakova, E., and Pacala, S. W.: A fire model with distinct crop, pasture, and non-agricultural burning: use of new data and a model-fitting algorithm for FINAL.1, Geosci. Model Dev., 11, 815–842, https://doi.org/10.5194/gmd-11-815-2018, 2018.

Reyer, C.P.O., Bathgate, S., Blennow, K., Borges, J.G., Bugmann, H., Delzon, S., Faias, S.P., Garcia-Gonzalo, J., Gardiner,

810

B., Gonzalez-Olabarria, J.R., Gracia, C., Hernández, J.G., and Kellomäki, S.: Are forest disturbances amplifying or canceling out climate change-induced productivity changes in European forests?, Environmental Research Letters, 12(3), 034027, 2017.

Scholten, R. C., Jandt, R., Miller, E. A., Rogers, B. M., and Veraverbeke, S.: Overwintering fires in boreal forests, Nature, 593, 399–404, 2021.

Seo, H., and Kim, Y.: Interactive impacts of fire and vegetation dynamics on global carbon and water budget using Community

815

Land Model version 4.5, Geoscientific Model Development, 12(1), 457–472, https://doi.org/10.5194/gmd-12-457-2019, 2019.

삭제함: .: Investigating the impact of agricultural fire management practices on the terrestrial carbon cycle, PhD thesis, Princeton University, Princeton, NJ, USA, available at: http://arks.princeton.edu/ark:/88435/dsp01k3569674p, 2016

16

820 Seo, H., and Kim, Y.: Global Fire Emissions Database burned-area dataset into Community Land Model version 5.0 – Biogeochemistry, Zenodo [code], https://zenodo.org/record/7483115, 2022.

Swezy, D. M. and Agee, J. K.: Prescribed-fire effects on fine-root and tree mortality in old-growth ponderosa pine, Can. J. Forest Res., 21, 626–634, https://doi.org/10.1139/x91-086, 1991.

Tarnocai, C., Kettles, I. M., and Lacelle, B.: Peatlands of Canada Map. Geological Survey of Canada, Open File 3834. Scale
825 1: 6 500 000, Natural Resources Canada, Ottawa, 2000.

Thonicke, K., Spessa, A., Prentice, I. C., Harrison, S. P., Dong, L., and Carmona-Moreno, C.: The influence of vegetation, fire spread and fire behaviour on biomass burning and trace gas emissions: Results from a process-based model, Biogeosciences, 7(6), 1991–2011, https://doi.org/10.5194/bg-7-1991-2010, 2010.

van der Werf, G. R., Randerson, J. T., Giglio, L., Collatz, G. J., Mu, M., Kasibhatla, P. S., Morton, D. C., Defries, R. S., Jin,
830 Y., and van Leeuwen, T. T.: Global fire emissions and the contribution of deforestation, savanna, forest, agricultural, and peat fires (1997-2009), Atmospheric Chemistry and Physics, 10(23), 11707–11735, https://doi.org/10.5194/acp-10-11707-2010, 2010.

Veraverbeke, S., Rogers, B. M., & Randerson, J. T.: Daily burned area and carbon emissions from boreal fires in Alaska, Biogeosciences, 12(11), 3579–3601, https://doi.org/10.5194/bg-12-3579-2015, 2015.

835 Veraverbeke, S., Rogers, B. M., Goulden, M. L., Jandt, R. R., Miller, C. E., Wiggins, E. B., & Randerson, J. T. (2017). Lightning as a major driver of recent large fire years in North American boreal forests, Nature Climate Change, 7(7), 529–534, https://doi.org/10.1038/nclimate3329, 2017.

Wang, Y., Cao, G., Wang, Y., Webb, A. A., Yu, P., and Wang, X.: Response of the daily transpiration of a larch plantation to variation in potential evaporation, leaf area index and soil moisture, Scientific Reports, 9(1), https://doi.org/10.1038/s41598-
840 019-41186-1, 2019.

Wu, Z., Li, M., Wang, B., Quan, Y., and Liu, J.: Using artificial intelligence to estimate the probability of forest fires in heilongjiang, Northeast China, Remote Sensing, 13(9), https://doi.org/10.3390/rs13091813, 2021.

Xiao, J. and Zhuang, Q.: Drought effects on large fire activity in Canadian and Alaskan forests, Environ. Res. Lett., 2, 044003, https://doi.org/10.1088/1748-9326/2/4/044003, 2007.
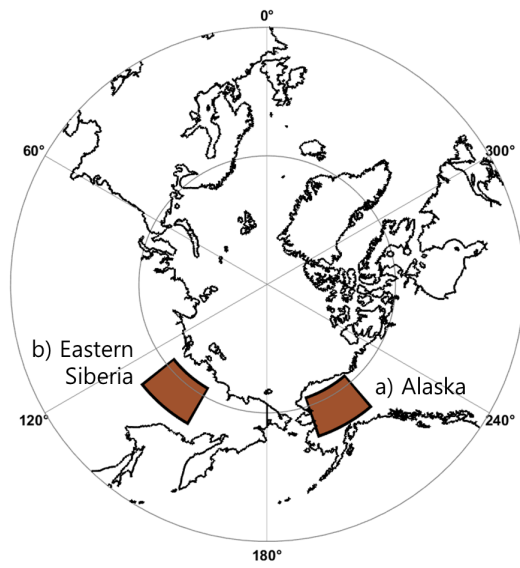
845

Figure 1. Study domain, (a) Alaska (200° E–218° E and 61° N–70° N), and (b) Eastern Siberia (130° E–149° E and 61° N–70° N).
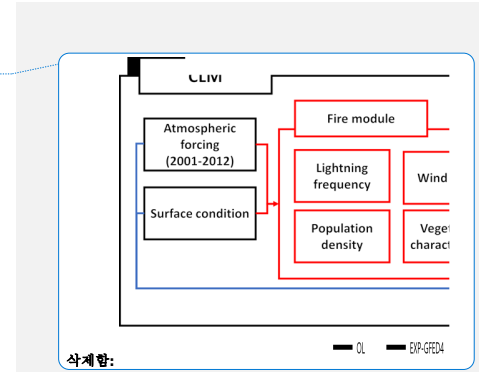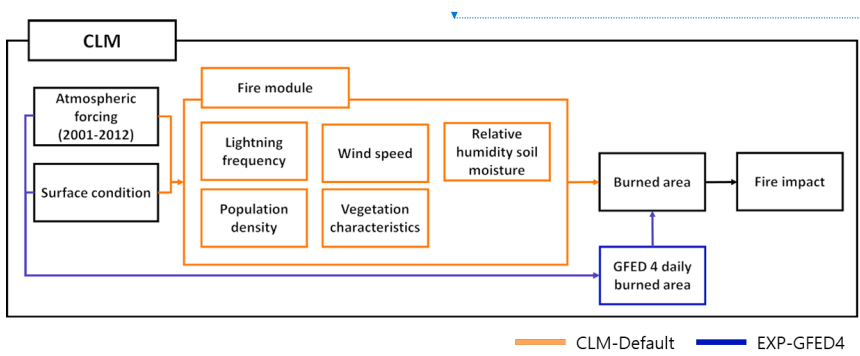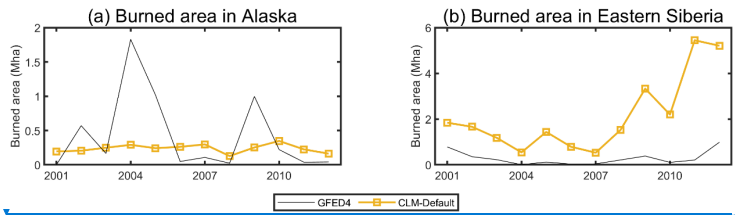
850

18

Figure 2. Flow diagram for CLM-Default (orange line) and EXP-GFED4 (blue line).

CLM-Default, default CLM5-BGC simulation; EXP-GFED4, experimental simulation with global fire emission database
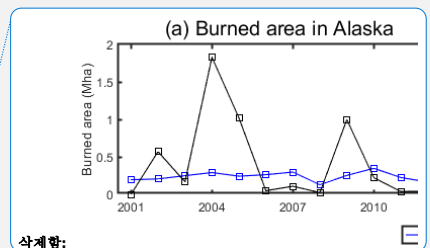
855

(a) Burned area in Alaska

(b) Burned area in Eastern Siberia

GFED4 — CLM-Default

Figure 3. Burned area based on GFED4 and simulated burned area of CLM-Default over (a) Alaska (b) and Eastern Siberia from 2001 to 2012.

GFED4, global fire emission database (version 4); OL, CLM-Default, default CLM5-BGC simulation

삭제함:

삭제함: **OL**

삭제함: open loop

서식 지정함: 글꼴 색: 검정, 영어(영국)
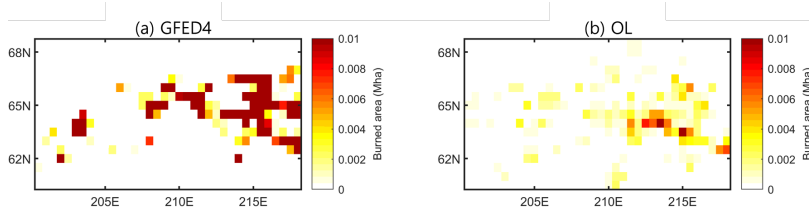
Figure 4. Spatial distribution of burned area of (a) GFED4 (b) and CLM-Default in 2004 over Alaska.

GFED4, global fire emission database (version 4); CLM-Default, default CLM5-BGC simulation

870
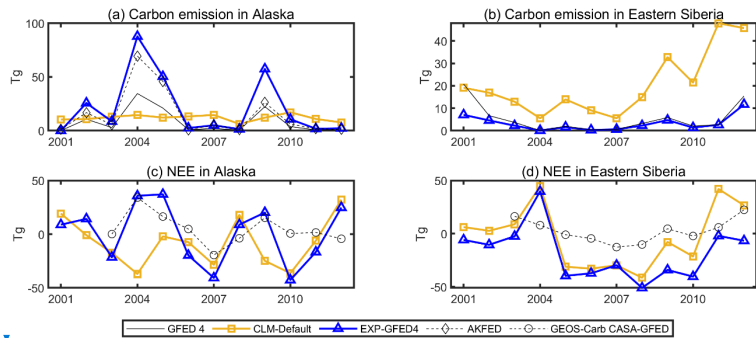
Figure 5. Simulated carbon fluxes of CLM-Default and EXP-GFED4 such as carbon emission (a,b), and (c,d) in Alaska (a,c) and Eastern Siberia (b,d) from 2001 to 2012. GFED carbon emission (a,b) and AKFED carbon emission (a) are added to evaluate the performance of carbon emission in CLM-Default and EXP-GFED4 runs. Also, NEE of GEOS-Carb CASA-GFED was added to evaluate the performance of NEE in CLM-Default and EXP-GFED4 runs (c, d).

CLM-Default, default CLM5-BGC simulation; EXP- GFED4, experimental simulation with global fire emission database (version 4); AKFED; Alaskan Fire Emissions Database; NEE, net ecosystem exchange.
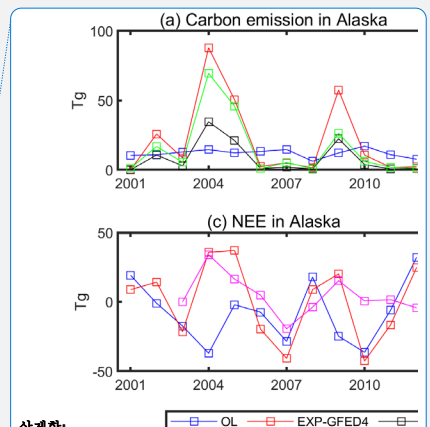
삭제함:
삭제함: OL (blue line)
삭제함: (red line)
삭제함: , black line
삭제함: , green line
삭제함: show
삭제함: impact
삭제함: burned assimilation to
삭제함: .
삭제함: OL
삭제함: , magenta line).
삭제함: OL, open loop
서식 지정함: 글꼴 색: 자동
서식 지정함: 영어(영국)
서식 지정함: 글꼴 색: 자동
서식 지정함: 글꼴 색: 자동
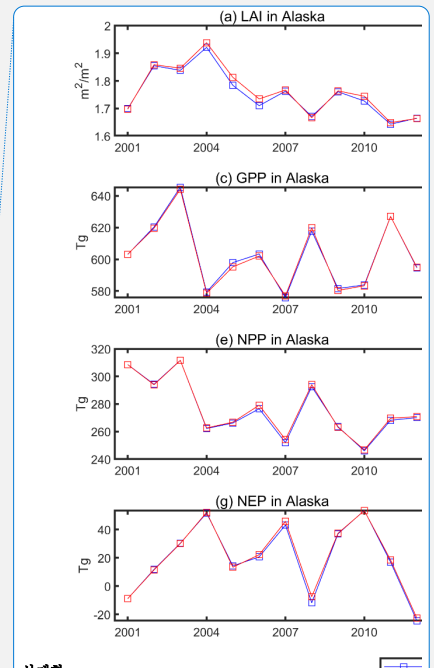서식 지정함: 글꼴: 9 pt
서식 지정함: 글꼴: 굵게 없음

Figure 6. Simulated LAI (a, b), and carbon fluxes of CLM-Default and EXP-GFED4 such as GPP (c, d), NPP (e, f), and NEP (g, h)
in Alaska (a, c, e, g) and Eastern Siberia (b, d, f, h) from 2001 to 2012.

LAI, leaf area index; CLM-Default, default CLM5-BGC simulation; EXP-GFED4, experimental simulation with global fire emission
database (version 4); GPP, gross primary production; NPP, net primary production; NEP, net ecosystem production
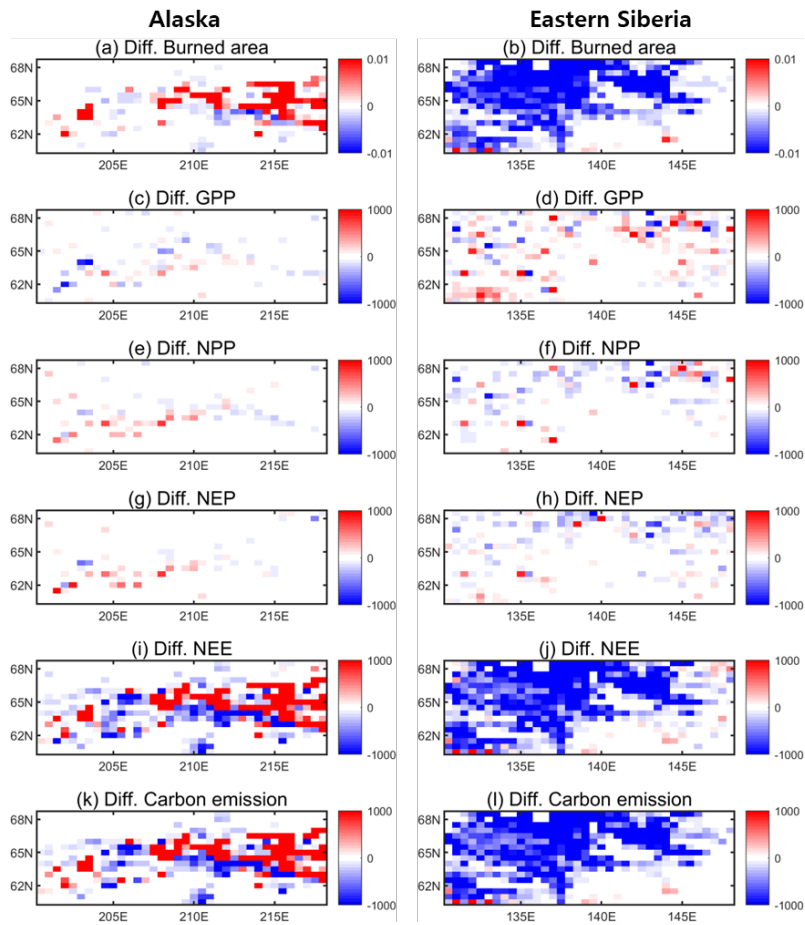
Figure 7. Map of difference of burned area (a,b) and carbon fluxes such as GPP (c,d), NPP (e,f), NEP (g,h), NEE (i,j), and carbon emission (k,l) in 2004 over Alaska (a,c,e,g,i,k) and in 2012 over Eastern Siberia (b,d,f,h,j,l).

GPP, gross primary production; NPP, net primary production; NEE, net ecosystem production
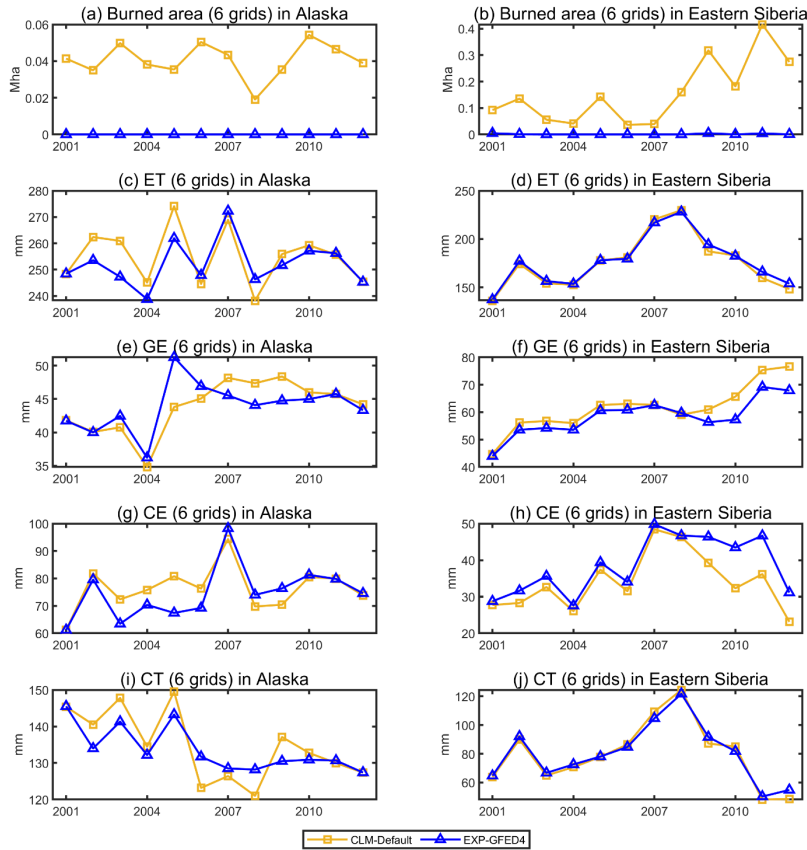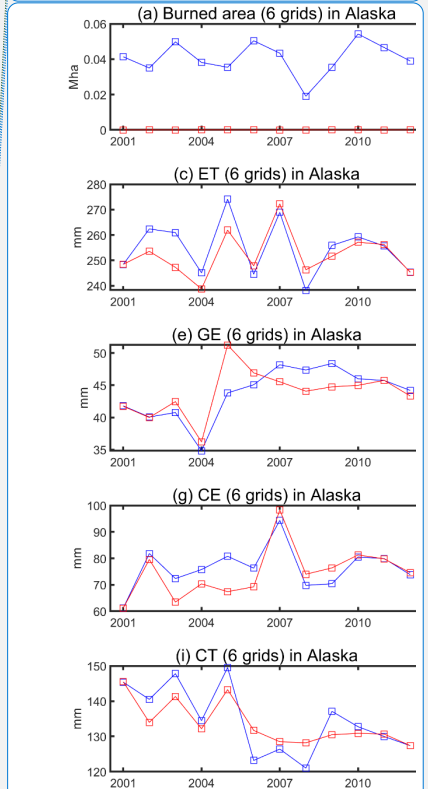
24

(a) GPP

(c) NEP

(e) Carbon emission
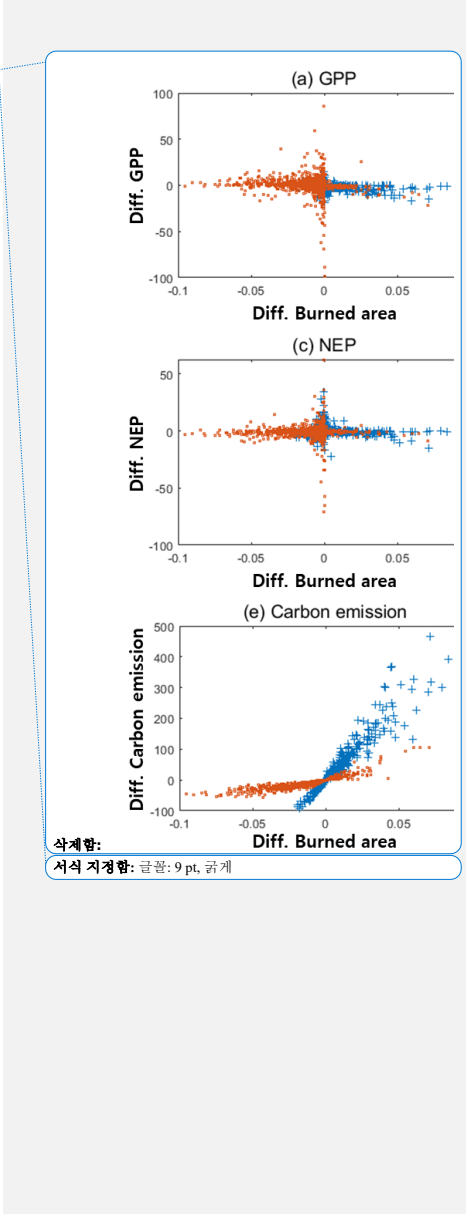
Figure 8. Simulated burned area (a, b), and water fluxes of CLM-Default and EXP-GFED4 such as ET (c, d), ground evaporation (GE; e, f), canopy evaporation (CE; g, h), and canopy transpiration (CT; i, j) in five grids where the difference in burned area between CLM-Default and EXP-GFED4 is highest in Alaska (a, c, e, g, i) and Eastern Siberia (b, d, f, h, j) from 2001 to 2012.

920 CLM-Default, default CLM5-BGC simulation; EXP-GFED4, experimental simulation with global fire emission database (version 4); ET, evapotranspiration.

(a) Differences in soil moisture in Alaska

(b) Differences in soil moisture in Eastern Siberia

Top soil   Bottom soil
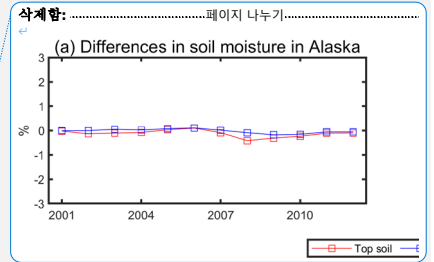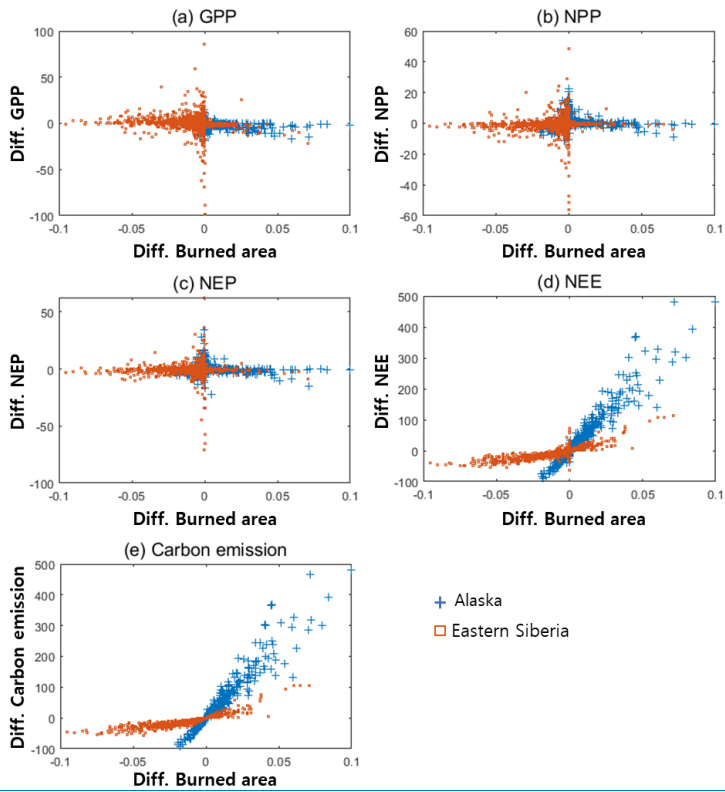
965

Figure 9. Differences (the value of OL- the value of EXP-GFED4) in simulated top soil (0–20 cm) moisture and bottom soil (70–150 cm) moisture in Alaska (a) and Eastern Siberia (b).

CLM-Default, default CLM5-BGC simulation; EXP-GFED4, experimental simulation with global fire emission database (version 4)

(a) GPP　　(b) NPP

(c) NEP　　(d) NEE

(e) Carbon emission

+ Alaska
□ Eastern Siberia

975　**Figure 10.** **The responses of the GPP (a), NPP (b), NEP (c), NEE (d), and carbon emission (e) to burned area over Alaska and Eastern Siberia.**

GPP, gross primary production; NPP, net primary production; NEP, net ecosystem production; NEE, net ecosystem production

[8] 이동함(삽입)

서식 지정함: 글꼴: 굵게

서식 지정함: 글꼴: 10 pt

Table 1. Model and data in this study.

Model	Domain and simulation period	Reference
Community Land Model 5 - Biogeochemistry	Alaska and Eastern Siberia (2001-2012)	Lawrence et al. (2019)

Data	Source	Reference
Burned area	GFED4	Giglio et al. (2013)
Carbon emission	GFED4	Giglio et al. (2013)
	AKFED	Veraverbeke et al. (2015)
NEE	GEOS-Carb CASA-GFED	Ott (2020)

GFED4, global fire emission database (version 4); NEE, net ecosystem exchange; AKFED, Alaskan Fire Emissions Database; GEOS-Carb CASA-GFED,

Table 2. Number of grid cells with more than 0.1 ha of burned area of GFED4 and CLM-Default.

Year	Number of grid cells (> 0.1Mha)	
	GFED v4	CLM-Default
2001	0	2
2002	21	1
2003	8	3
2004	51	2
2005	38	1
2006	2	3
2007	3	2
2008	0	0
2009	31	1
2010	7	3
2011	0	3
2012	1	2

GFED4, global fire emission database (version 4); CLM-Default, default CLM5-BGC simulation

Table 3. Simulated carbon fluxes; carbon emission, GPP, NPP, NEP, and NEE in CLM-Default and CLM-GFED over Alaska and Eastern Siberia.

Units (gC/m²/year)	Alaska		Eastern Siberia	
	CLM-Default	EXP-GFED4	CLM-Default	EXP-GFED4
Carbon emission	11.87	21.12	20.48	3.24
GPP	602.51	602.12	405.16	406.14
NPP	276	276.79	201.2	199.49
NEP	19.5	20.42	23.28	21.56
NEE	-7.63	0.7	-2.79	-18.32

995 GPP, gross primary production; NPP, net primary production; NEP, net ecosystem production; NEE, net ecosystem exchange; CLM-Default, default CLM5-BGC simulation; EXP-GFED4, experimental simulation with global fire emission database

삭제함: OL

삭제함: OL

삭제함: OL, open loop

Table 4. Carbon emission of CLM-Default, EXP-GFED4, GFED4 and AKFED from 2001 to 2012 over Alaska.

Carbon emission (g/m2/year)	CLM-Default	EXP-GFED4	GFED 4	AKFED
2001	10.37	0.05	0.04	1.16
2002	10.77	25.71	10.63	16.76
2003	12.85	8.59	2.88	5.48
2004	14.53	87.81	34.56	69.43
2005	12.18	50.43	21.02	45.78
2006	13.22	2.44	0.97	0.82
2007	14.62	4.97	2.03	5.26
2008	6.20	1.38	0.54	0.87
2009	12.10	57.49	22.32	26.30
2010	17.09	10.62	3.74	6.02
2011	10.89	1.79	0.72	1.86
2012	7.64	2.19	0.88	1.21
Average	11.87	21.12	8.36	15.08

CLM-Default, default CLM5-BGC simulation; EXP-GFED4, experimental simulation with global fire emission database; AKFED; Alaskan Fire Emissions Database

005

페이지 5: [1] 삭제함 authors 2023. 6. 10. PM 2:18:00

페이지 7: [2] 삭제함 authors 2023. 6. 10. PM 2:18:00

페이지 7: [3] 삭제함 authors 2023. 6. 10. PM 2:18:00

페이지 9: [4] 삭제함 authors 2023. 6. 10. PM 2:18:00

페이지 9: [5] 삭제함 authors 2023. 6. 10. PM 2:18:00

페이지 9: [6] 삭제함 authors 2023. 6. 10. PM 2:18:00

페이지 23: [7] 서식 지정함 authors 2023. 6. 10. PM 2:18:00
글꼴 색: 사용자 지정 색(RGB(4,50,255)), 영어(미국)

페이지 23: [7] 서식 지정함 authors 2023. 6. 10. PM 2:18:00
글꼴 색: 사용자 지정 색(RGB(4,50,255)), 영어(미국)

페이지 23: [7] 서식 지정함 authors 2023. 6. 10. PM 2:18:00
글꼴 색: 사용자 지정 색(RGB(4,50,255)), 영어(미국)

페이지 23: [8] 서식 지정함 authors 2023. 6. 10. PM 2:18:00
글꼴 색: 사용자 지정 색(RGB(4,50,255)), 영어(미국)

페이지 23: [8] 서식 지정함 authors 2023. 6. 10. PM 2:18:00
글꼴 색: 사용자 지정 색(RGB(4,50,255)), 영어(미국)

페이지 23: [8] 서식 지정함 authors 2023. 6. 10. PM 2:18:00
글꼴 색: 사용자 지정 색(RGB(4,50,255)), 영어(미국)

페이지 23: [8] 서식 지정함 authors 2023. 6. 10. PM 2:18:00
글꼴 색: 사용자 지정 색(RGB(4,50,255)), 영어(미국)

페이지 23: [8] 서식 지정함 authors 2023. 6. 10. PM 2:18:00
글꼴 색: 사용자 지정 색(RGB(4,50,255)), 영어(미국)

페이지 26: [15] 서식 지정함   authors   2023. 6. 10. PM 2:18:00

글꼴 색: 사용자 지정 색(RGB(4,50,255)), 영어(미국)

페이지 26: [16] 서식 지정함   authors   2023. 6. 10. PM 2:18:00

글꼴 색: 사용자 지정 색(RGB(4,50,255)), 영어(미국)

페이지 26: [16] 서식 지정함   authors   2023. 6. 10. PM 2:18:00

글꼴 색: 사용자 지정 색(RGB(4,50,255)), 영어(미국)

페이지 26: [17] 서식 지정함   authors   2023. 6. 10. PM 2:18:00

글꼴 색: 사용자 지정 색(RGB(4,50,255)), 영어(미국)

페이지 26: [17] 서식 지정함   authors   2023. 6. 10. PM 2:18:00

글꼴 색: 사용자 지정 색(RGB(4,50,255)), 영어(미국)

페이지 26: [18] 서식 지정함   authors   2023. 6. 10. PM 2:18:00

글꼴 색: 사용자 지정 색(RGB(4,50,255)), 영어(미국)

페이지 26: [18] 서식 지정함   authors   2023. 6. 10. PM 2:18:00

글꼴 색: 사용자 지정 색(RGB(4,50,255)), 영어(미국)

페이지 26: [19] 서식 지정함   authors   2023. 6. 10. PM 2:18:00

글꼴 색: 사용자 지정 색(RGB(4,50,255)), 영어(미국)

페이지 26: [20] 서식 지정함   authors   2023. 6. 10. PM 2:18:00

글꼴 색: 사용자 지정 색(RGB(4,50,255)), 영어(미국)

페이지 26: [20] 서식 지정함   authors   2023. 6. 10. PM 2:18:00

글꼴 색: 사용자 지정 색(RGB(4,50,255)), 영어(미국)

페이지 26: [21] 서식 지정함   authors   2023. 6. 10. PM 2:18:00

글꼴 색: 사용자 지정 색(RGB(4,50,255)), 영어(미국)

페이지 26: [22] 서식 지정함   authors   2023. 6. 10. PM 2:18:00

글꼴 색: 사용자 지정 색(RGB(4,50,255)), 영어(미국)

페이지 26: [22] 서식 지정함   authors   2023. 6. 10. PM 2:18:00

글꼴 색: 사용자 지정 색(RGB(4,50,255)), 영어(미국)

페이지 26: [22] 서식 지정함   authors   2023. 6. 10. PM 2:18:00

글꼴 색: 사용자 지정 색(RGB(4,50,255)), 영어(미국)

페이지 26: [22] 서식 지정함   authors   2023. 6. 10. PM 2:18:00

글꼴 색: 사용자 지정 색(RGB(4,50,255)), 영어(미국)

페이지 26: [22] 서식 지정함   authors   2023. 6. 10. PM 2:18:00

글꼴 색: 사용자 지정 색(RGB(4,50,255)), 영어(미국)

페이지 26: [22] 서식 지정함   authors   2023. 6. 10. PM 2:18:00

글꼴 색: 사용자 지정 색(RGB(4,50,255)), 영어(미국)

페이지 26: [22] 서식 지정함   authors   2023. 6. 10. PM 2:18:00

글꼴 색: 사용자 지정 색(RGB(4,50,255)), 영어(미국)

페이지 26: [22] 서식 지정함   authors   2023. 6. 10. PM 2:18:00

글꼴 색: 사용자 지정 색(RGB(4,50,255)), 영어(미국)

페이지 26: [22] 서식 지정함   authors   2023. 6. 10. PM 2:18:00

글꼴 색: 사용자 지정 색(RGB(4,50,255)), 영어(미국)

페이지 26: [23] 서식 지정함   authors   2023. 6. 10. PM 2:18:00

글꼴 색: 자동, 영어(미국)

페이지 26: [23] 서식 지정함   authors   2023. 6. 10. PM 2:18:00

글꼴 색: 자동, 영어(미국)

페이지 26: [23] 서식 지정함   authors   2023. 6. 10. PM 2:18:00

글꼴 색: 자동, 영어(미국)

페이지 26: [23] 서식 지정함   authors   2023. 6. 10. PM 2:18:00

글꼴 색: 자동, 영어(미국)

페이지 26: [23] 서식 지정함   authors   2023. 6. 10. PM 2:18:00

글꼴 색: 자동, 영어(미국)

페이지 26: [23] 서식 지정함   authors   2023. 6. 10. PM 2:18:00

글꼴 색: 자동, 영어(미국)

페이지 26: [23] 서식 지정함   authors   2023. 6. 10. PM 2:18:00

글꼴 색: 자동, 영어(미국)